SANDIA REPORT

SAND2015-xxx
Unlimited Release
Printed June 2015

A Modified Gurson Model: Formulation and Implementation

Jakob T. Ostien, Qiushi Chen

Prepared by
Sandia National Laboratories
Albuquerque, New Mexico 87185 and Livermore, California 94550

Sandia National Laboratories is a multi-program laboratory managed and operated by Sandia Corporation, a wholly owned subsidiary of Lockheed Martin Corporation, for the U.S. Department of Energy's National Nuclear Security Administration under contract DE-AC04-94AL85000.

Approved for public release; further dissemination unlimited.

Sandia National Laboratories

Issued by Sandia National Laboratories, operated for the United States Department of Energy by Sandia Corporation.

NOTICE: This report was prepared as an account of work sponsored by an agency of the United States Government. Neither the United States Government, nor any agency thereof, nor any of their employees, nor any of their contractors, subcontractors, or their employees, make any warranty, express or implied, or assume any legal liability or responsibility for the accuracy, completeness, or usefulness of any information, apparatus, product, or process disclosed, or represent that its use would not infringe privately owned rights. Reference herein to any specific commercial product, process, or service by trade name, trademark, manufacturer, or otherwise, does not necessarily constitute or imply its endorsement, recommendation, or favoring by the United States Government, any agency thereof, or any of their contractors or subcontractors. The views and opinions expressed herein do not necessarily state or reflect those of the United States Government, any agency thereof, or any of their contractors.

Printed in the United States of America. This report has been reproduced directly from the best available copy.

Available to DOE and DOE contractors from
U.S. Department of Energy
Office of Scientific and Technical Information
P.O. Box 62
Oak Ridge, TN 37831

Telephone: (865) 576-8401
Facsimile: (865) 576-5728
E-Mail: reports@adonis.osti.gov
Online ordering: http://www.osti.gov/bridge

Available to the public from
U.S. Department of Commerce
National Technical Information Service
5285 Port Royal Rd
Springfield, VA 22161

Telephone: (800) 553-6847
Facsimile: (703) 605-6900
E-Mail: orders@ntis.fedworld.gov
Online ordering: http://www.ntis.gov/help/ordermethods.asp?loc=7-4-0#online

SAND2015-xxx
Unlimited Release
Printed June 2015

A Modified Gurson Model: Formulation and Implementation

Jakob T. Ostien
Mechanics of Materials
Sandia National Laboratories
P.O. Box 969
Livermore, CA 94551
jtostie@sandia.gov

Qiushi Chen
Glenn Department of Civil Engineering
Clemson University
Clemson, SC 29634
qiushi@clemson.edu

Abstract

In this report a modified Gurson modeled is presented. It can be used to model ductile behavior up to and including material failure. The formulation incorporates the Gurson failure surface, including void nucleation, growth, and coalescence, with a J_2 yield surface including user-defined hardening behavior. Details of the formulation and implementation into Sierra/SolidMecahnics are discussed, and some pertinent aspects and features of the model are illustrated through a select few numerical examples.

Contents

List of Figures

List of Tables

Chapter 1

Introduction

The purpose of this work is to present a modified Gurson constitutive model used in capturing the behavior of ductile materials up to and including the failure regime. The original Gurson model was developed by [4] based on rigorous micromechanical analysis of a characteristic volume element with spherical or cylindrical-shaped voids surrounded by rigid plastic matrix material. This model was motivated by experimental observations of dilational plastic deformation during ductile fracture in porous metals, which generate considerable porosity due to the nucleation and growth of voids. Tvergaard and Needleman [14] later improved the original Gurson model by introducing additional parameters into the yield function and by introducing an effective void volume fraction term to account for coalescence of voids that more accurately captured the void volume fraction growth rates. This model is referred to as the 'Gurson-Tvergaard-Needleman' or the GTN model.

One important limitation of the original Gurson or the GTN model is that the void growth (i.e., the damage) depends only on the mean stress. In a shear-dominated state, such as in a projectile penetration problem, the model is unable to predict damage growth if continuous void nucleation is not invoked. This limitation motivates a modification of the original void growth law to include a shear term proposed in [7]. This modification, though phenomenological in nature, has been shown to improve the prediction of the Gurson model in situations where shear stress dominates [7, 8].

The original Gurson model and the recently introduced shear modification were both formulated either with a small deformation assumption or within a hypoelastic framework. The large deformation setting typically encountered in a ductile failure simulation would render the small deformation formulation inappropriate. As for the hypoelastic formulation, there are well known drawbacks such as the non-zero work done in a closed cycle of elastic deformation, which violates the most important axiom of an elastic response [1].

To avoid the above problems, in Section 2, the shear-modified Gurson model in [7, 8] will be reformulated within a large deformation hyperelastic constitutive framework. Since the elastic response is derived from a hyperelastic potential, the work done in a closed elastic deformation loop vanishes exactly. Furthermore, the hyperelastic formulation eliminates the need for incrementally objective stress update algorithms and can be easily integrated with frame-invariant formulations of anisotropic elasticity and anisotropic plastic yielding [1]. The

scope of the current work, however, is limited to an isotropic treatment.

The remainder of this report includes a discussion of the model formulation in Chapter 2 and a discussion of the implementation in Chapter 3. Chapter 4 showcases a select few numerical examples of the model. Chapter 5 finishes with a conclusions and a discussion of the efficacy of the model.

Chapter 2

Model Formulation

This section should begin with a short description about the origins of the model, including the desire to capture porous solid behavior related to void growth with an inelastic body. Then some comments about the thermodynamic motivation to place it within a hyperelastic framework. It should include sections on the flow rule and each piece of the void volume fraction evolution equation.

This chapter discusses in detail the physical and mathematical formulation of the modified Gurson model under investigation. It begins with kinematic preliminaries and expresses the hyperelastic constitutive relation. The yield function is defined in combination with a hardening law and flow rule. Then the evolution equations for the void volume fraction and presented, as per the porous solid assumption.

2.1 Preliminaries for large deformation hyperelastic formulation

2.1.1 Kinematic preliminaries

To set the stage for the hyperelastic formulation, the kinematic preliminaries for large deformation elastoplasticity are summarized in this section, along with the quantities and relations that will be used in subsequent model development.

An essential feature of this elastoplasticity framework is the multiplicative decomposition of the deformation gradient $\boldsymbol{F}$ into an elastic part $\boldsymbol{F}^e$ and a plastic part $\boldsymbol{F}^p$

$$\boldsymbol{F} = \boldsymbol{F}^e \cdot \boldsymbol{F}^p. \tag{2.1}$$

This decomposition introduces the notion of an intermediate local configuration (cf. [11] and the references therein for the motivation and micromechanical basis for such a decomposition).

Next, we introduce a set of strain measures associated with the multiplicative decomposition that will be used extensively in the model development. First is the right Cauchy-Green tensor $\boldsymbol{C}$, and its plastic counterpart $\boldsymbol{C}^p$, which are defined in the reference configuration

$$\boldsymbol{C} = \boldsymbol{F}^T \cdot \boldsymbol{F} \tag{2.2}$$

$$\boldsymbol{C}^p = \boldsymbol{F}^{pT} \cdot \boldsymbol{F}^p \tag{2.3}$$

where $\boldsymbol{F}^T$ is the transpose of $\boldsymbol{F}$.

In the current configuration we consider the left Cauchy-Green tensor $\boldsymbol{b}$, and its elastic counterpart $\boldsymbol{b}^e$

$$\boldsymbol{b} = \boldsymbol{F} \cdot \boldsymbol{F}^T \tag{2.4}$$

$$\boldsymbol{b}^e = \boldsymbol{F}^e \cdot \boldsymbol{F}^{eT} \tag{2.5}$$

The above fundamental strain measures are related via pull-back and push-forward operations

$$\boldsymbol{C}^{-p} = \boldsymbol{F}^{-1} \cdot \boldsymbol{b}^e \cdot \boldsymbol{F}^{-T} \tag{2.6}$$

$$\boldsymbol{b}^e = \boldsymbol{F} \cdot \boldsymbol{C}^{-p} \cdot \boldsymbol{F}^T \tag{2.7}$$

In metal plasticity, a standard assumption is that plastic flow is isochoric (volume-preserving), i.e. $\det(\boldsymbol{F}^p) = 1$, which implies

$$J = \det(\boldsymbol{F}) = \det(\boldsymbol{F}^e) \tag{2.8}$$

Defining $J^e = \det(\boldsymbol{F}^e)$, we have the volume preserving part of the elastic left Cauchy-Green tensor $\bar{\boldsymbol{b}}^e$

$$\bar{\boldsymbol{b}}^e = J^{e^{-2/3}} \boldsymbol{b}^e = J^{-2/3} \boldsymbol{b}^e. \tag{2.9}$$

2.1.2 Hyperelastic constitutive relation

The starting point of the hyperelastic constitutive formulation is the assumption of the existence of a strain-energy function, which is proposed to have the following form

$$\Psi = \Psi^{\text{vol}}[J^e] + \Psi^{\text{iso}}[\bar{\boldsymbol{b}}^e] \tag{2.10}$$

Here the strain-energy function Ψ is a decoupled function of the volumetric part (i.e., $J^e = \det \boldsymbol{F}^e$) and the isochoric part (i.e., $\bar{\boldsymbol{b}}^e$) of the elastic deformation. The volumetric and the isochoric parts of the strain-energy function are given as

$$\Psi^{\text{vol}}[J^e] = \frac{\kappa}{4}\left(J^{e2} - 1 - \ln\, \mathrm{J}^{\mathrm{e}2}\right) \tag{2.11}$$

$$\Psi^{\text{iso}}[\bar{\boldsymbol{b}}^e] = \frac{\mu}{2}\left(\mathrm{tr}(\bar{\boldsymbol{b}}^{\mathrm{e}}) - 3\right) \tag{2.12}$$

where κ and μ are the bulk and shear modulus. Here we are following the developments of ([13]), however we employ a different choice of strain energy-functions. The elastic constitutive law and the Kirchhoff stresses are given as

$$\boldsymbol{\tau} = J^e p\mathbf{1} + \boldsymbol{s} \tag{2.13}$$

The Kirchhoff pressure p and the deviatoric stress tensor $\boldsymbol{s}$ are related to the elastic strain measure as

$$p = \frac{1}{3}\,\mathrm{tr}(\boldsymbol{\tau}) = \frac{\kappa}{2}\left(J^{e2} - 1\right)/J^e \tag{2.14}$$

$$\boldsymbol{s} = \mathrm{dev}(\boldsymbol{\tau}) = \mu\,\mathrm{dev}(\bar{\boldsymbol{b}}^e) \tag{2.15}$$

2.2 Constitutive relations of the Gurson model

Within the previously described large deformation hyperelastic framework, key components of the constitutive relations of the shear-modified Gurson model are presented in this section, including the yield function, the hardening law, the flow rule and the evolution law for the shear-modified void growth.

2.2.1 Yield function

The yield function Φ of the Gurson model can be written in terms of the previously defined Kirchhoff mean stress p and deviatoric stress tensor $\boldsymbol{s}$ as

$$\Phi = \frac{1}{2}\boldsymbol{s} : \boldsymbol{s} - \frac{1}{3}\psi Y^2 \tag{2.16}$$

where ψ contains contributions from the damage in the material and Y is the Kirchhoff yield stress. This yield function (2.16) is a quadratic version form. This particular variant of the yield function was chosen as it proved to exhibit superior properties of robustness in convergence in the nonlinear solution algorithm outline below.

The function ψ directly relates to the void volume fraction of the porous solid and is given as

$$\psi = 1 + q_3 f^2 - 2q_1 f \cosh(v), \quad v = \frac{3q_2 p}{2Y} \tag{2.17}$$

where p is the Kirchhoff pressure defined in (2.14), and f is the void volume fraction of the porous solid. The Kirchhoff yield stress Y describes the hardening of the undamaged matrix material. Also, the constants $q_1, q_2 2, q_3$ are the accepted additional yield parameters often present in GTN type models.

2.2.2 Hardening law

The hardening law relates the yield strength Y to some measure of plastic deformation. One example of a nonlinear hardening law proposed by [11] for metal is written as

$$Y = Y_0 + Y_\infty \left[1 - \exp(-\delta \varepsilon_q)\right] + K\varepsilon_q \tag{2.18}$$

where ε_q is the equivalent plastic strain, Y_0 is the initial yield strength, Y_∞ is the residual flow stress, K is the hardening coefficient, and δ is the saturation exponent. Other forms of hardening law can also be used depending on the observed material behavior.

The plastic work increment in the matrix material is equal to the macroscopic plastic work increment, which can be used to derive the evolution equation for the equivalent plastic strain ε_q as

$$\dot{\varepsilon}_q Y(1-f) = \boldsymbol{\tau} : \left(\gamma \frac{\partial \Phi}{\partial \boldsymbol{\tau}}\right) \tag{2.19}$$

Substituting yield function Φ into (2.19) to obtain the expression to compute $\dot{\varepsilon}_q$

$$\dot{\varepsilon}_q = \frac{1}{1-f}\left(\gamma \sqrt{\frac{2|\psi|}{3}} \operatorname{sign}(\psi) + \frac{pt}{Y}\right) \tag{2.20}$$

2.2.3 Flow rule

Following the standard procedure of the principle of maximum dissipation, Simo and Miehe [10] proposed a general form of associate flow rule, which is adopted in the current formulation and is given as

$$-\frac{1}{2}L_v(\boldsymbol{b}^e)\cdot\boldsymbol{b}^{-e}=\gamma\frac{\partial\Phi}{\partial\boldsymbol{\tau}}=\gamma\boldsymbol{n}+\frac{1}{3}t\mathbf{1} \tag{2.21}$$

where $L_v(\boldsymbol{b}^e)=\boldsymbol{F}\cdot\dot{\boldsymbol{C}}^{-p}\cdot\boldsymbol{F}^T$ is the Lie derivative, and $\boldsymbol{n}$ and t are the deviatoric and volumetric component of the gradient term, respectively. Substituting the yield function (2.16) leads to the following

$$\boldsymbol{n}=\frac{\boldsymbol{s}}{\|\boldsymbol{s}\|} \tag{2.22}$$

$$t=\operatorname{tr}\left(\gamma\frac{\partial\Phi}{\partial\boldsymbol{\tau}}\right)=\sqrt{\frac{3}{2}}\gamma f\sinh(\frac{3p}{2Y})\frac{1}{\sqrt{|\psi|}}\operatorname{sign}(\psi) \tag{2.23}$$

2.2.4 Evolution of void volume fraction

The void volume fraction f is the internal variable that characterizes the material damage. The rate of change in total void volume fraction, $\dot{f}$, is typically given by the sum of contributions due to the void growth, $\dot{f}_g$, and the nucleation of new voids, $\dot{f}_n$.

$$\dot{f}=\dot{f}_g+\dot{f}_n \tag{2.24}$$

In the original Gurson model [4], the void growth part $\dot{f}_g$ was related to the plastic volume change as

$$\dot{f}_g=(1-f)\operatorname{tr}\left(\gamma\frac{\partial\Phi}{\partial\boldsymbol{\tau}}\right) \tag{2.25}$$

To account for the void growth under shear-dominated stress state, the void growth law (2.25) was extended in [7] by adding a term that depends on the third stress invariant. This shear-modified void growth equation is written as

$$\dot{f}_g=(1-f)\operatorname{tr}\left(\gamma\frac{\partial\Phi}{\partial\boldsymbol{\tau}}\right)+k_\omega f\frac{\omega(\boldsymbol{\tau})}{\tau_e}\boldsymbol{s}:\left(\gamma\frac{\partial\Phi}{\partial\boldsymbol{\tau}}\right) \tag{2.26}$$

where $\tau_e = \sqrt{3/2}\|\boldsymbol{s}\|$ is the effective deviatoric Kirchhoff stress, k_ω is a material constant that sets the magnitude of the damage growth rate in pure shear states [7]. The function $\omega(\boldsymbol{\tau})$ includes the effect of the third stress invariant on void growth and is given as

$$\omega(\boldsymbol{\tau}) = 1 - \left(\frac{27 J_3}{2\tau_e^3}\right)^2 \tag{2.27}$$

where $J_3 = \det(\boldsymbol{s})$ is the third invariant of deviatoric Kirchhoff stress tensor.

Substituting the yield function (2.16) and the expression for $\omega(\boldsymbol{\tau})$ (2.27) into the void growth law (2.26) yields

$$\dot{f}_g = (1-f)t + \sqrt{\frac{2}{3}}\gamma k_\omega f \omega(\boldsymbol{\tau}) \tag{2.28}$$

The effective increase in damage due to plastic strain controlled nucleation is given by [3] as

$$\dot{f}_{nu} = A\dot{\varepsilon}_q \tag{2.29}$$

where the parameter A is defined as a function of the matrix equivalent plastic strain ε_q

$$A = \begin{cases} \frac{f_N}{s_N\sqrt{2\pi}} \exp\left[-\frac{1}{2}\left(\frac{\varepsilon_q - \epsilon_N}{s_N}\right)^2\right], & p \geq 0 \\ 0, & p < 0 \end{cases} \tag{2.30}$$

where the nucleation strain follows a normal distribution with a mean value ϵ_N and a standard deviation s_N with the volume fraction of the nucleated voids given by f_N.

Chapter 3

Implementation

This section should discuss implementation aspects of the large deformation hyperelastic model and the implicit integration scheme. I based the Sierra implementation off of the Albany version, so that would be a good place to start. In both places we are using Sacado to compute derivative for the local consistent tangent, so we should talk about what that buys us.

Details of the numerical implementation of the large deformation hyperelastic Gurson model are discussed in this section. A fully implicit integration scheme ([11, 13]) is implemented to integrate the flow rule, the evolution equation for the internal variable (e.g., ε_q), and the evolution equation for the void volume fraction f over a finite time step $\Delta t = t_{n+1} - t_n$. The integration scheme consists of an elastic trial state followed by a plastic correction. Stresses and the internal variables are updated at time t_{n+1} given their known values at time t_n and the deformation gradient $\boldsymbol{F}_{n+1}$.

The implicit integration scheme results a set of nonlinear discrete equations for integrating the stress and internal variables, which requires an iterative solution method such as the Newton's method. In the Newton's method, precise derivatives are necessary to assemble the local Jacobian matrix that is essential to achieve an optimal asymptotic convergence rate. In this work, a technique called the forward automatic differentiation (FAD) will be used to compute necessary derivatives. The implementation will leverage the existing FAD capability of the Sacado package in Sandia National Laboratories' Trilinos framework [5].

3.1 Discrete form of the rate equations

To derive the discrete form of the rate equations, the starting point is to write the evolution equations in the material (reference) configuration. For the flow rule, a pull-back operation is applied to (2.21) such that

$$-\frac{1}{2}\dot{\boldsymbol{C}}^{-p}\cdot\boldsymbol{C}^{p} = \gamma\boldsymbol{F}^{-1}\cdot\frac{\partial\Phi}{\partial\boldsymbol{\tau}}\cdot\boldsymbol{F} \tag{3.1}$$

where γ is the plastic multiplier. Then, the application of the exponential mapping to (3.1) yields an incremental objective integration algorithm

$$\boldsymbol{C}_{n+1}^{-p} = \boldsymbol{F}_{n+1}^{-1} \cdot \exp\left(-2\Delta\gamma \frac{\partial \Phi_{n+1}}{\partial \boldsymbol{\tau}}\right) \cdot \boldsymbol{F}_{n+1} \cdot \boldsymbol{C}_{n}^{-p} \tag{3.2}$$

Applying the push-forward operation to (3.2) yields an update algorithm for the elastic left Cauchy-Green tensor $\boldsymbol{b}_{n+1}^{e}$ as

$$\boldsymbol{b}_{n+1}^{e} = \exp\left(-2\Delta\gamma \frac{\partial \Phi_{n+1}}{\partial \boldsymbol{\tau}}\right) \cdot \boldsymbol{b}^{e\,\mathrm{tr}} \tag{3.3}$$

where the trial elastic left Cauchy-Green tensor $\boldsymbol{b}^{e\,\mathrm{tr}}$ is given by

$$\boldsymbol{b}^{e\,\mathrm{tr}} = \boldsymbol{F}_{n+1} \cdot \boldsymbol{C}_{n}^{-p} \cdot \boldsymbol{F}_{n+1}^{T} \tag{3.4}$$

From elastic and plastic isotropy, $\boldsymbol{b}_{n+1}^{e}, \boldsymbol{b}^{e\,\mathrm{tr}}$ and $\boldsymbol{\tau}$ have identical principal axes. Then, the logarithmic Hencky strains follow as

$$\ln \boldsymbol{b}_{n+1}^{e} = \ln \boldsymbol{b}^{e\,\mathrm{tr}} - 2\Delta\gamma \frac{\partial \Phi_{n+1}}{\partial \boldsymbol{\tau}} \tag{3.5}$$

Using the elastic constitutive relations (2.14) and (2.15), the Kirchhoff pressure and deviatoric stress tensor at time t_{n+1} can be obtained as

$$p_{n+1} = p^{\mathrm{tr}} - \kappa t \tag{3.6}$$

$$\boldsymbol{s}_{n+1} = \boldsymbol{s}^{\mathrm{tr}} - 2\mu\Delta\gamma\boldsymbol{n} \tag{3.7}$$

where $\boldsymbol{n}$ and t are given by (2.22), (2.23) and are evaluated at time t_{n+1}, and p^{tr} and $\boldsymbol{s}^{\mathrm{tr}}$ are the trial states given by

$$p^{\mathrm{tr}} = \kappa \ln J^{e\,\mathrm{tr}}, \quad J^{e\,\mathrm{tr}} = \det(\boldsymbol{b}^{e\,\mathrm{tr}})^{1/2} \tag{3.8}$$

$$\boldsymbol{s}^{\mathrm{tr}} = \mu\, \mathrm{dev} \ln \boldsymbol{b}^{e\,\mathrm{tr}} \tag{3.9}$$

The discrete form of evolution equations for internal variable ε_q and the void volume fraction f are obtained by apply backward Euler scheme to their evolution equations (2.24) and (2.20). The resulting discrete equations are

$$f_{n+1} = f_n + (1 - f_{n+1})t + \sqrt{\frac{2}{3}}\Delta\gamma k_\omega f_{n+1}\omega(\boldsymbol{\tau}) + A_{n+1}(\varepsilon_{q(n+1)} - \varepsilon_{q(n)}) \tag{3.10}$$

$$\varepsilon_{q(n+1)} = \varepsilon_{q(n)} + \frac{1}{1 - f_{n+1}}\left(\Delta\gamma\sqrt{\frac{2|\psi|}{3}}\mathrm{sign}(\psi) + \frac{p_{n+1}t}{Y}\right) \tag{3.11}$$

3.2 Local nonlinear system of equations

The discrete form of the rate equations (3.3), (3.6), (3.7), (3.10) and (3.11) include four unknowns quantities relate to the stresses and internal state variables at time t_{n+1}, which are the pressure p, the equivalent plastic strain ε_q, the void volume fraction f, and the plastic multiplier $\Delta\gamma$.

The unknowns will be obtained from solving the following nonlinear system of equations. For simplicity, in the following, we will omit the index $n+1$ referring to the current time t_{n+1}. The resulting nonlinear system of equations are

$$R_1(\boldsymbol{X}) = \|\boldsymbol{s}^{\mathrm{tr}}\| - 2\mu\Delta\gamma - \sqrt{\frac{2}{3}}\mathrm{sign}(\psi)\sqrt{|\psi|}Y \tag{3.12}$$

$$R_2(\boldsymbol{X}) = p - p^{\mathrm{tr}} + \kappa t \tag{3.13}$$

$$R_3(\boldsymbol{X}) = f - f_n - (1-f)t - \sqrt{\frac{2}{3}}\Delta\gamma k_\omega f\omega(\boldsymbol{\tau}) - A(\varepsilon_q - \varepsilon_{q(n)}) \tag{3.14}$$

$$R_4(\boldsymbol{X}) = \varepsilon_q - \varepsilon_{q(n)} - \frac{1}{1-f}\left(\Delta\gamma\sqrt{\frac{2|\psi|}{3}}\mathrm{sign}(\psi) + \frac{pt}{Y}\right) \tag{3.15}$$

where, the vector of unknowns $\boldsymbol{X}$ is

$$\boldsymbol{X} = \{p, f, \varepsilon_q, \Delta\gamma\} \tag{3.16}$$

The above nonlinear system of equations can be solved through iterative solution method such as the Newton's method. The implicit algorithm for integrating the shear-modified large deformation Gurson model is summarized in the following box.

Box 1. Implicit algorithm for integrating shear-modified large deformation Gurson model

GIVEN: $\varepsilon_{q(n)}, f_n, \boldsymbol{b}_n^e$ and $\boldsymbol{F}$
FIND: $\boldsymbol{\tau}, \varepsilon_q, f, \boldsymbol{b}^e$(or $\boldsymbol{F}^p$) at time t_{n+1}
STEP 1. Compute trial elastic left Cauchy-Green tensor $\boldsymbol{b}_e^{\text{tr}}$ (3.4)
STEP 2. Compute trial stresses $p^{\text{tr}}, \boldsymbol{s}^{\text{tr}}$ (3.8), (3.9)
STEP 3. Check yielding (2.16): $\Phi^{\text{tr}}(p^{\text{tr}}, \boldsymbol{s}^{\text{tr}}, \varepsilon_{q(n)}, f_n) > 0$?
No, set $p = p^{\text{tr}}, \boldsymbol{s} = \boldsymbol{s}^{\text{tr}}, \boldsymbol{b}^e = \boldsymbol{b}^{e\,\text{tr}}, \varepsilon_q = \varepsilon_{q(n)}, f = f_n$ and exit
STEP 4. Yes, local Newton loop
4.1 Initialize $\boldsymbol{X}^k$ (3.16) and the iteration count $k = 0$
4.2 Assemble the residual equations $\boldsymbol{R}(\boldsymbol{X}^k)$ (3.12) - (3.15)
4.3 Check convergence: $\| \boldsymbol{R} \| < tolerance$?
Yes, converged and go to STEP 5
4.4 No, compute local Jacobian matrix $\boldsymbol{J} = \partial \boldsymbol{R} / \partial \boldsymbol{X}$
4.5 Solve system of equations $\boldsymbol{J} \cdot \delta \boldsymbol{X} = \boldsymbol{R}$ for $\delta \boldsymbol{X}$
4.6 Update $\boldsymbol{X}^{k+1} = \boldsymbol{X}^k - \delta \boldsymbol{X}$, $k \to k+1$ and go to 4.2
STEP 5. Update $\boldsymbol{\tau} = \boldsymbol{s} + p\boldsymbol{g}$, ε_q, f, and $\boldsymbol{F}^p$

The plastic deformation gradient $\boldsymbol{F}^p$, which is used in (3.1) and (3.4) to compute trial state, is updated using

$$\boldsymbol{F}^p = \exp\left(\frac{\partial \Phi}{\partial \boldsymbol{\tau}}\right) \cdot \boldsymbol{F}_n^p \tag{3.17}$$

In the Newton's iterative solution method, it requires consistent linearization of the system of equation (3.12) - (3.15), which necessities a derivative of the objective functions with respect to the independent fields (i.e., the unknowns). The Jacobian derivative of the objective function ($\boldsymbol{J} = \partial \boldsymbol{R} / \partial \boldsymbol{X}$) is commonly referred to as the algorithmic consistent tangent operator in the constitutive model literature [6, 12]. In this work, a technique in computational science called the forward automatic differentiation (FAD) will be used to compute necessary derivatives. FAD provides an efficient and convenient way to evaluate derivatives. It will be detailed in the next section. Interested readers can also refer to [2] for applications of FAD to constitutive modeling in small- and large-deformation computational inelasticity.

3.3 FAD: a numerical exact way of computing consistent tangent

The FAD technique is applied towards computing the tangent operator ($\boldsymbol{J} = \partial \boldsymbol{R} / \partial \boldsymbol{X}$) which involves first- and second- derivatives of the local system of residual equations (3.12)- (3.15), with respect to the unknown vector (3.16). The implementation is presented in Sandia National Laboratories' Albany analysis code[9], which utilizes the Sacado package contained in Sandia's Trilinos framework to supply the automatic differentiation capabilities employed. To utilize the FAD technique for computing the local tangent operator, one must template

both the system of residual equations and unknown vectors in terms of a Sacado FAD type data instead of the typical double precision data type. The unknown *state vector* will be the independent variable, while the residual equations will be generic functions dependent on the state vectors. The FAD data type contains not only the value of the data but also the derivative of the data with respect to the independent variables. The derivative information is initialized appropriately and propagated forward through the algorithm. In this way, once the sensitivities are initialized , the Jacobian or tangent operator will be calculated automatically. AD is also employed in the Albany analysis code to form the global system Jacobian, or stiffness matrix, for solving boundary value problems.

Chapter 4

Numerical Examples

This section could be renamed to Numerical Examples, and should include any and all verification/validation work. To be clear, for the purpose of the SAND report, we don't require any validation. I will have to include a description of the Sierra input parameters for use in their user's manual, but obviously I'll worry about that.

To demonstrate the model, the plasticity parameters were fit to data obtained from the tensile testing of an A286 alloy. Subsequently, some of the parameters governing the failure behavior of the model were varied to study their effects. The data collection and parameter fitting details are outside of the scope of this report, and the results of this process can be seen in Figure 4.1 and Table 4.1, where the ranges of the relevant parameters are listed as appropriate for the study. Note that in Figure 4.1, as for other multi-linear hardening models in Sierra, the `YIELD_STRESS` parameter aligns with the first non-zero true strain point in the curve.

4.1 Uniaxial Tension

In this section we investigate the behavior of the model in a state of uniaxial tension. In particular, we will observe the stress and void volume fraction response for a variety of failure parameter combinations to develop an understanding of the behavior of the model. Figure 4.2 shows the model behavior for various values of the shear parameter k_ω, and evidently it has little to no effect on the response for this stress state.

In Figure 4.3 a set of nucleation parameters are specified and also evaluated in the uniaxial tension scenario. In this case the volume fraction of nucleated voids f_N, is varied, while the mean value and standard deviation of failure strain, ϵ_N and s_N respectively, are specified and held constant. Observe that the von Mises stress component is somewhat reduced, to a greater extent as the volume fraction of nucleated voids is increased. Also observe that the void volume fraction grows by approximately the specified volume fraction of nucleated voids, accelerated the apparent void growth until the total void volume fraction of nucleated void has been exhausted. Afterwards, the trajectory returns to that of the void growth

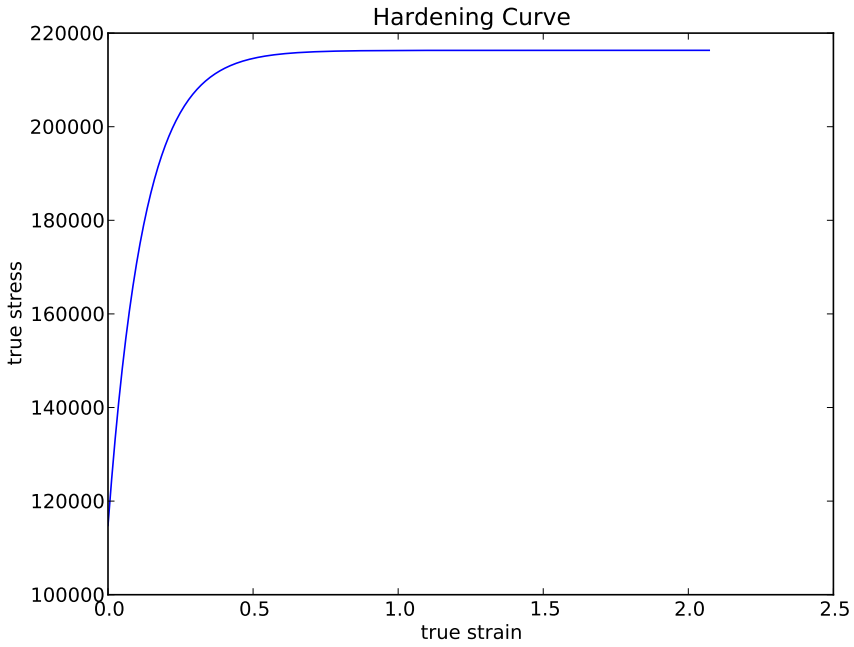

Figure 4.1. True stress versus true strain, obtained from a fitting the tensile behavior of an A286 steel alloy.

Parameters	
YOUNGS_MODULUS	29.0e6 *psi*
POISSONS_RATIO	0.3
YIELD_STRESS	1.14794e5 *psi*
Q1	1.5
Q2	1.0
Q3	2.25
KW	{0,5,10}
INITIAL_VOID	{0.0001,0.001,0.01}
EN	{0.0,0.1,0.2}
SN	0.1
FN	{0.0,0.1,0.2}
CRITICAL_VOID	0.5
FAILURE_VOID	0.6667
HARDENING_FUNCTION	see Figure 4.1

Table 4.1. Input parameters for the Gurson model in Sierra and the ranges over which parameters were varied in the present study.

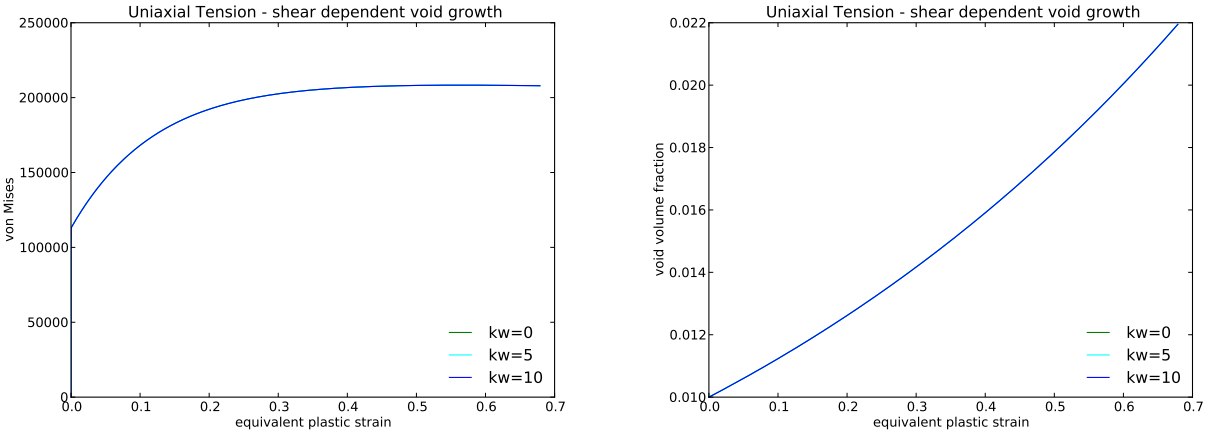

(a) stress

(b) void volume fraction

Figure 4.2. Von Mises stress component and void volume fraction plotted against equivalent plastic strain. The shear void growth parameter has an insignificant effect on the response of the material point in tension.

without augmentation.

4.2 Simple Shear

In this section we investigate the behavior of the two components of the failure model, specifically the shear dependent void growth and the void nucleation terms, in the context of simple shear. To test this problem we use the plasticity parameters developed in the previous section and study the response of the model to with various failure parameters. In Figure 4.4 we vary the shear parameter, k_ω, which governs the rate of void growth in shear dominated states of stress as per (2.26). Observe that in the extreme case for simple shear k_ω can accelerate void growth to the point of complete material failure corresponding to the shear stress component reaching a value of zero.

In Figure 4.5 a set of nucleation parameters are specified and also evaluated in the simple shear scenario. In this case the volume fraction of nucleated voids f_N, is varied, while the mean value and standard deviation of failure strain, ϵ_N and s_N respectively, are specified and held constant. Observe that the shear stress component is somewhat reduced, to a greater extent as the volume fraction of nucleated voids is increased. Also observe that the void

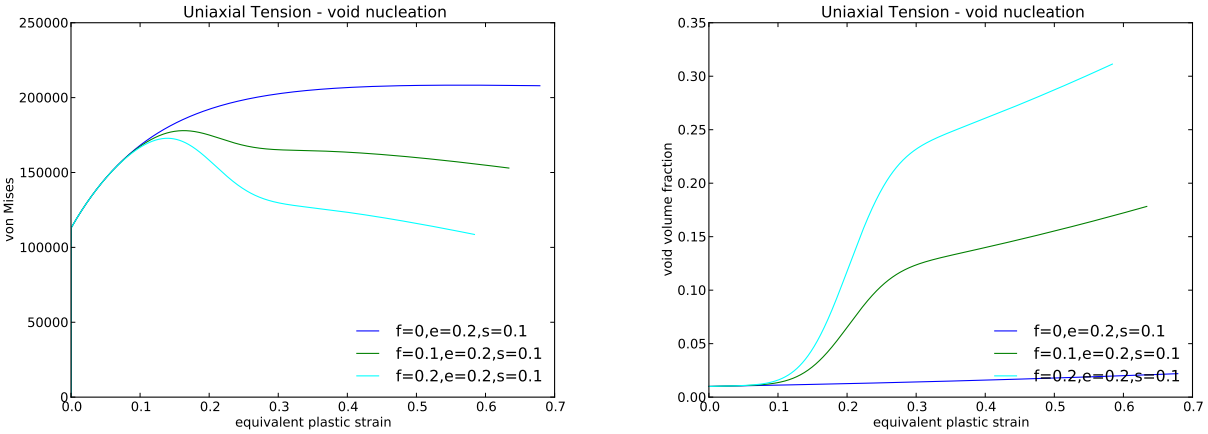

(a) stress

(b) void volume fraction

Figure 4.3. Von Mises component and void volume fraction plotted against equivalent plastic strain. The void nucleation parameters have some effect on the response of the material point in uniaxial tension.

volume fraction grows by approximately the specified volume fraction of nucleated voids, in particular, where f_N is zero, the void volume fraction does not deviate from zero.

4.3 Shear Compression

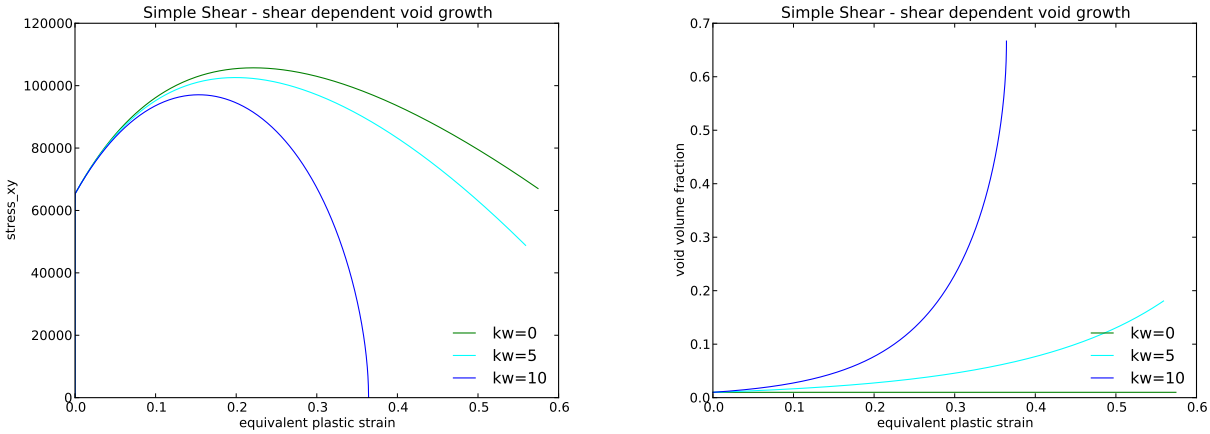

(a) stress

(b) void volume fraction

Figure 4.4. Shear stress component and void volume fraction plotted against equivalent plastic strain. The shear void growth parameter has a pronounced effect on the response of the material point in simple shear.

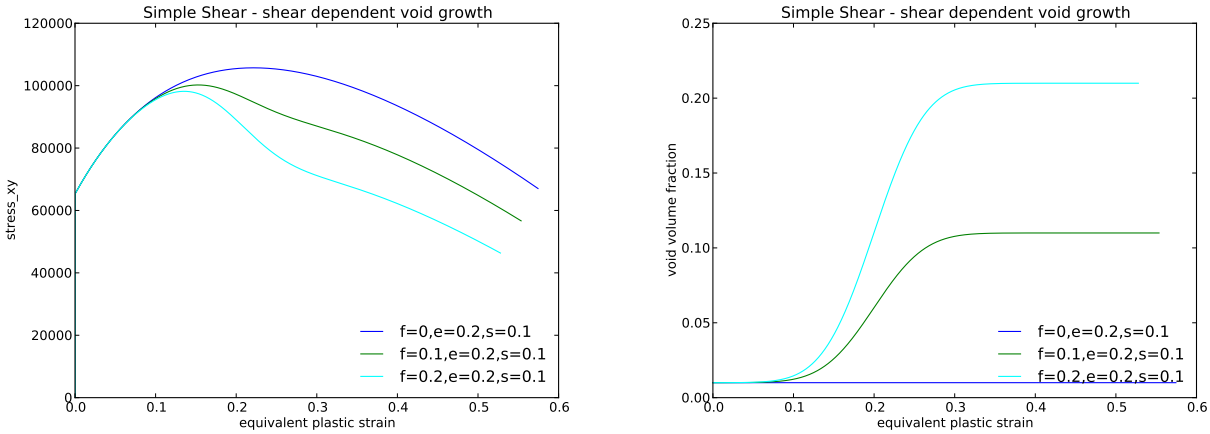

(a) stress

(b) void volume fraction

Figure 4.5. Shear stress component and void volume fraction plotted against equivalent plastic strain. The void nucleation parameters have some effect on the response of the material point in simple shear.

Chapter 5

Conclusions

This should be a summary and short discussion about the strengths and weaknesses of the model. Nothing too fancy, just practice for the journal article.

References

[1] Belytschko, T., Liu, W. K., Moran, B., Elkhodary, K., 2013. Nonlinear finite elements for continua and structures. John Wiley & Sons.

[2] Chen, Q., Ostien, J. T., Hansen, G., et al., 2014. Automatic differentiation for numerically exact computation of tangent operators in small-and large-deformation computational inelasticity. In: TMS 2014 143rd Annual Meeting & Exhibition, Annual Meeting Supplemental Proceedings. John Wiley & Sons, p. 289.

[3] Chu, C., Needleman, A., 1980. Void nucleation effects in biaxially stretched sheets. Journal of Engineering Materials and Technology(Transactions of the ASME) 102 (3), 249–256.

[4] Gurson, A. L., 1977. Continuum theory of ductile rupture by void nucleation and growth: Part iâĂŤyield criteria and flow rules for porous ductile media. Journal of engineering materials and technology 99 (1), 2–15.

[5] Heroux, M., Bartlett, R., Hoekstra, V. H. R., Hu, J., Kolda, T., Lehoucq, R., Long, K., Pawlowski, R., Phipps, E., Salinger, A., et al., 2003. An overview of trilinos. Tech. rep., Technical Report SAND2003-2927, Sandia National Laboratories.

[6] Miehe, C., 1996. Numerical computation of algorithmic (consistent) tangent moduli in large-strain computational inelasticity. Computer Methods in Applied Mechanics and Engineering 134 (3), 223–240.

[7] Nahshon, K., Hutchinson, J., 2008. Modification of the gurson model for shear failure. European Journal of Mechanics-A/Solids 27 (1), 1–17.

[8] Nahshon, K., Xue, Z., 2009. A modified gurson model and its application to punch-out experiments. Engineering fracture mechanics 76 (8), 997–1009.

[9] Salinger, A. G., Bartett, R. A., Chen, Q., Gao, X., Hansen, G., Kalashnikova, I., Mota, A., Muller, R. P., Nielsen, E., Ostien, J., et al., 2013. Albany: A component-based partial differential equation code built on trilinos. Tech. rep., Sandia National Laboratories Livermore, CA; Sandia National Laboratories (SNL-NM), Albuquerque, NM (United States).

[10] Simo, J., Miehe, C., Jul. 1992. Associative coupled thermoplasticity at finite strains: Formulation, numerical analysis and implementation. Computer Methods in Applied Mechanics and Engineering 98 (1), 41–104.

[11] Simo, J. C., Hughes, T. J. R., 1998. Computational Inelasticity. Springer Verlag.

[12] Simo, J. C., Taylor, R. L., 1985. Consistent tangent operators for rate-independent elastoplasticity. Computer Methods in Applied Mechanics and Engineering 48 (1), 101–118.

[13] Steinmann, P., Miehe, C., Stein, E., 1994. Comparison of different finite deformation inelastic damage models within multiplicative elastoplasticity for ductile materials. Computational Mechanics 13 (6), 458–474.

[14] Tvergaard, V., Needleman, A., 1984. Analysis of the cup-cone fracture in a round tensile bar. Acta metallurgica 32 (1), 157–169.

DISTRIBUTION:

1 Qiushi Chen
Clemson University, Lowry Hall 109
Clemson, SC 29634

1 MS 9042 Jake Ostien, 8256

1 MS 9042 James W. Foulk III, 8256

1 MS ???? Kendall Pierson, 1542

1 MS 0899 Technical Library, 8944 (electronic copy)


Sandia National Laboratories